Quantification of Feeding Effects of Spot Feeding Ductile Iron castings made in Vertically Parted Molds

N.K. Vedel-Smith, N.S. Tiedje
Technical University of Denmark, Kgs. Lyngby, Denmark

J. Sällström
FOSECO Sweden, Åmål, Sweden

K.T. Maza
Vald.Birn A/S, Holstebro, Denmark

ABSTRACT

In vertically parted molds it is traditionally difficult to feed heavy sections that cannot be reached by traditional side/top feeders or other conventional methods. This project aims at quantifying the effects of using molded-in ram-up spot feeders as a means of feeding isolated sections in castings made in vertically parted molds and it gives directions towards the effectiveness of this technology.

The casting examined is a disc-shaped casting with an inner boss and an outer ring, separated by a thin walled section. Thus, both boss and ring are prone to porosities.

The experimental work analyses the effect of different exothermic and insulating spot feeders and their interaction with traditional parting line feeders, with respect to porosities and surface shrinkage. Experiments were performed using EN-GJS-500-7 and EN-GJS-450-10 alloys.

The experiment shows that the geometry cannot be cast successfully without the use of both a top and a spot feeder. Leaving out one or both feeders, results in porosities and surface shrinkage. For EN-GJS-500-7 any combination with both feeders present produced sound castings. For the more demanding EN-GJS-450-10 the exothermic spot feeder produced sound castings. All other combinations displayed some degree of porosities.

Keywords: Spot feeding, porosities, surface shrinkage, ductile iron, sleeves, ram-up sleeves, vertically parted molds, porosity

INTRODUCTION

As the price of energy is rising, and will continue to rise in coming years, melt reduction has become a significant parameter with which to improve a foundry's business. It has been shown that great savings in raw materials,

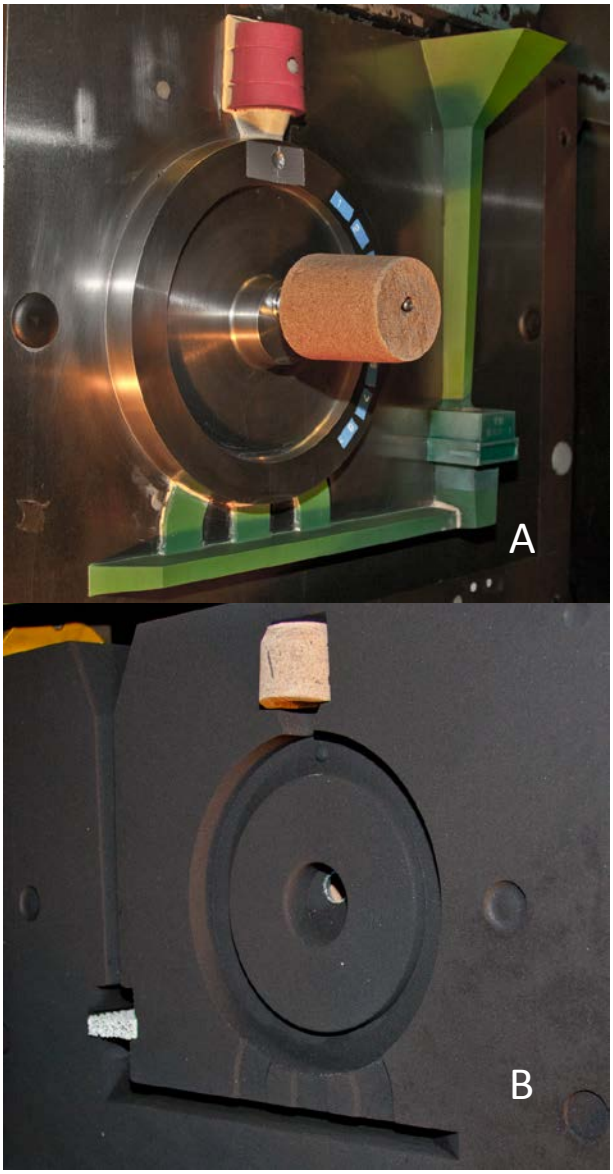

Fig. 1. A) Pattern plate with gating system (green), top feeder geometry (red), the casting geometry and pin with Ram-Up Sleeve (at the center). B) Molded in Ram-Up Sleeve spot feeder (center), 10 PPI foam filter and top feeder sleeve.

energy and money can be achieved by optimizing feeding methods[1]. Proper feeding of the castings gives an improved yield, which in return saves energy for melting, and thus money.

While there still may be room for further optimization of traditional feeders, the larger gains are achieved by new approaches to the feeding challenge. New opportunities present themselves to the designer of the cast layout, enabling otherwise difficult castings to be produced with a profit.

Spot feeders, on vertically parted molds, enable feeding of areas located away from the parting line of the mold, much like the feeder placement known from horizontally parted molds. The spot feeders are sleeves of insulating or exothermic material, or a combination material. They provide melt and heat for the chosen area, thus changing the overall thermal gradients of the casting and the local direction of solidification.

This paper is the result of an ongoing project, involving several companies, working towards characterizing, quantifying and understanding the effect of various feeder applications.

Ram-Up Sleeves

The spot feeder is molded into the sand mold using the ram-up sleeve system. The sleeve is made of exothermic, insulating or a combined exothermic-insulating material. Traditionally sleeves are inserted into the molded sand on vertically parted molds. The ram-up sleeves, though, are mounted onto a specially designed pin which holds the sleeve in place while the mold is compacted. The pin is placed on the pattern at the location where the feeder is to be located. See fig. 1.

The ram-up sleeves have a collapsible steel neck, which enable them to collapse and compact the sand around the feeder neck while protecting the sleeve itself during the molding operation.

The solution with the ram-up pin enables the feeder to be placed away from the parting line, making it possible to apply spot feeders on vertically parted molds. Only major restriction is that the ram-up pin and sleeve must be aligned with the direction of mold compression.

EXPERIMENTAL SETUP

THE CASTING GEOMETRY

The test geometry used for this experiment consists of a disc with an inner boss and an outer ring, separated by a thin plate like section. The geometry is designed to display casting problems similar to those found on disc-brakes, fly-wheels and other castings with higher modulus sections, isolated from feeding by in between low modulus sections. See fig. 2. The casting's design dimensions can be found in table 1 alongside the calculated modulus and feed modulus for the different sections of the casting.

$$M_f = 1.2 \cdot M_c \qquad \text{Eq. 1}$$

where M_c is the modulus of the casting section in question calculated as volume divided by cooling area[2].

Table 1. Casting Geometry Dimensions and Modulus [mm]. Section overview found in fig. 3.

	III	IV	V	VI	VII
Height	25	55	50	55	25
Thickness	20	10	30	10	20
Modulus	6	5	9	5	6
Feed Modulus	7	6	11	6	7

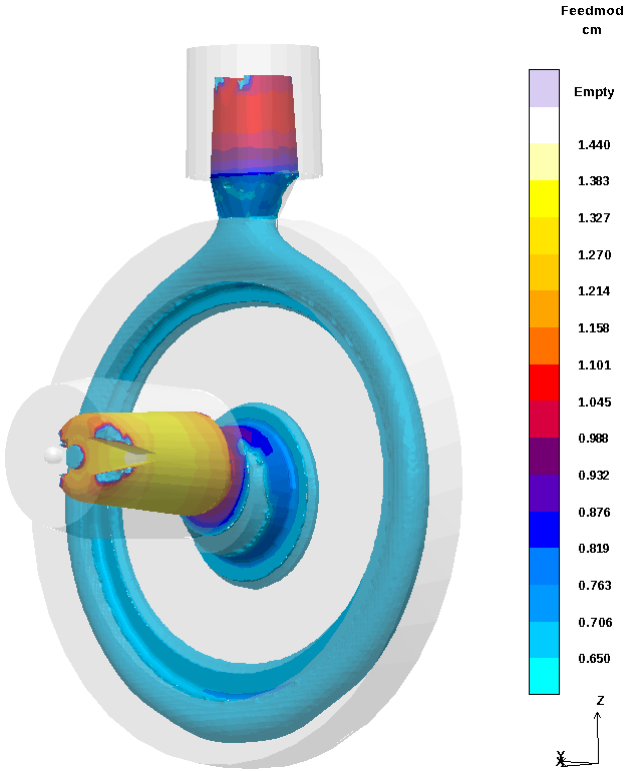

Fig. 2. Feeding modulus for casting geometry. The out ring and inner boss show higher modulus than the section in between. The highest modulus is found in the feeders, with the center feeder as the greater.

The downsprue, runner and gating design are all of conventional design. A 10 PPI[1] foam filter was placed at the bottom of the downsprue to reduce turbulence and capture inclusions in the melt. See fig. 1.

The poured weight is approx. 8 kg and the casting itself weighs 4 kg.

[1] Pores Per Inch

ALLOYS

Two different cast irons were used in the experiment. The first alloy was a traditional EN-GJS-500-7[3] (α), which is a commonly used cast iron with little shrinkage. The other alloy was a EN-GJS-450-10[3] (β) with high silicon content, displaying close to fully ferritic structure with better elongation and machinability. The alloys chemical compositions are shown in table 2.

Table 2. Alloy Compositions [wt%]

	C	Si	Mn	P	S	Mg	Cu
EN-GJS-500-7 (α)	3.67	2.73	0.50	0.015	0.005	0.049	0.025
EN-GJS-450-10 (β)	3.35	3.48	0.34	0.017	0.003	0.046	0.010

The lower carbon content makes the alloy more prone to shrinkage and porosity defects.

Both alloys are near eutectic, and are as such expected to solidify in a similar manner. Thus, the main difference between the alloys can be contributed to the higher C content and thus greater graphite expansion of the EN-GJS-500-7 alloy.

FEEDER SLEEVES

The experiment made it possible to vary the thermal (or true) modulus (M_t) without changing the geometric modulus (M_g).

$$M_g = \frac{V}{A} \qquad \text{Eq. 2}$$

Thus, the results are free from changes in hydrostatic pressure caused by a larger liquid volume, but retain the effects related to solidification time.

The sleeve material provides a Modulus Extension Factor[2] (MEF) which is material specific. The MEF is an addition to the geometric modulus. The MEF is determined by the material properties and the geometry—i.e. thickness—of the sleeve walls.

All feeders have the same geometric modulus. Thus, they cannot be meaningfully compared based on this figure alone. Instead the different feeder sleeves are compared using the thermal modulus[2].

$$M_t = \text{MEF} \cdot M_g \qquad \text{Eq. 3}$$

Feeder Placement

The casting is designed with two feeders—1) a top feeder placed on top of the outer ring at the mold parting line, and 2) a center feeder placed away from the parting line using a Ram-Up Sleeve. The top feeders used here were made from either insulating (M_t 9 mm) or exothermic and insulating (M_t 10 mm) material. The center feeder sleeves were made from exothermic (M_t 12 mm), insulating (M_t 11 mm) or a mixture of exothermic/insulating (M_t 11 mm) materials.

Feeder Combinations

The trials comprised 18 combinations of feeders and cast-alloys. However, this paper only presents data from 8 of these trials. The 8 triplicate casting groups are systematically numbered from α1-5 for the EN-GJS-500-7 alloy, and β1-3 for the EN-GJS-450-10 alloy. Each triplicate copy is denoted A, B or C.

The feeder combinations examined here are show in table 3. The combinations are designed to give insight into the effect of the different feeder types, as well as the absence of the one or both feeders.

Table 3. Feeder Combinations. Exo stands for exothermic, Ins stands for insulating and E/I stands for exothermic-insulating.

	α1	α2	α3	α4	α5	β1	β2	β3
Top	E/I	Ins	E/I	-	-	E/I	Ins	E/I
Center	Exo	Ins	-	E/I	-	Exo	Ins	-

Castings α1-5 were cast with EN-GJS-500-7 alloy, whereas β1-3 were cast with the EN-GJS-450-10 alloy.

CASTING CONDITIONS

The trials were made under production conditions at Vald.Birn Iron Foundry A/S in Holstebro, Denmark. The experimental castings were cast using a vertical molding line—DISAMATIC 2013. The castings were made during two separate trials in June 2011 and January 2012. Both experiments used the same vertical molding line with identical machine settings for each trial. All molds were green sand molds.

All castings were made using a heated pouring station, keeping the melt temperature constant between the first and the last poured casting. The castings were cast in three sequences; 1st and 2nd in June 2011 with the EN-GJS-500-7 alloy. First sequence was cast at 1,401±5 °C (2,554±10 °F). Second sequence was cast within an hour of the first sequence, and was cast at 1,408±5 °C (2,566±10 °F). The 3rd and final sequence was cast in January 2012 with the EN-GJS-450-10 alloy at 1,392±5 °C (2,538±10 °F). The chemical composition shown in table 2 was determined with optical emission spectroscopy. The pouring times for all castings were approx. 3.5 s.

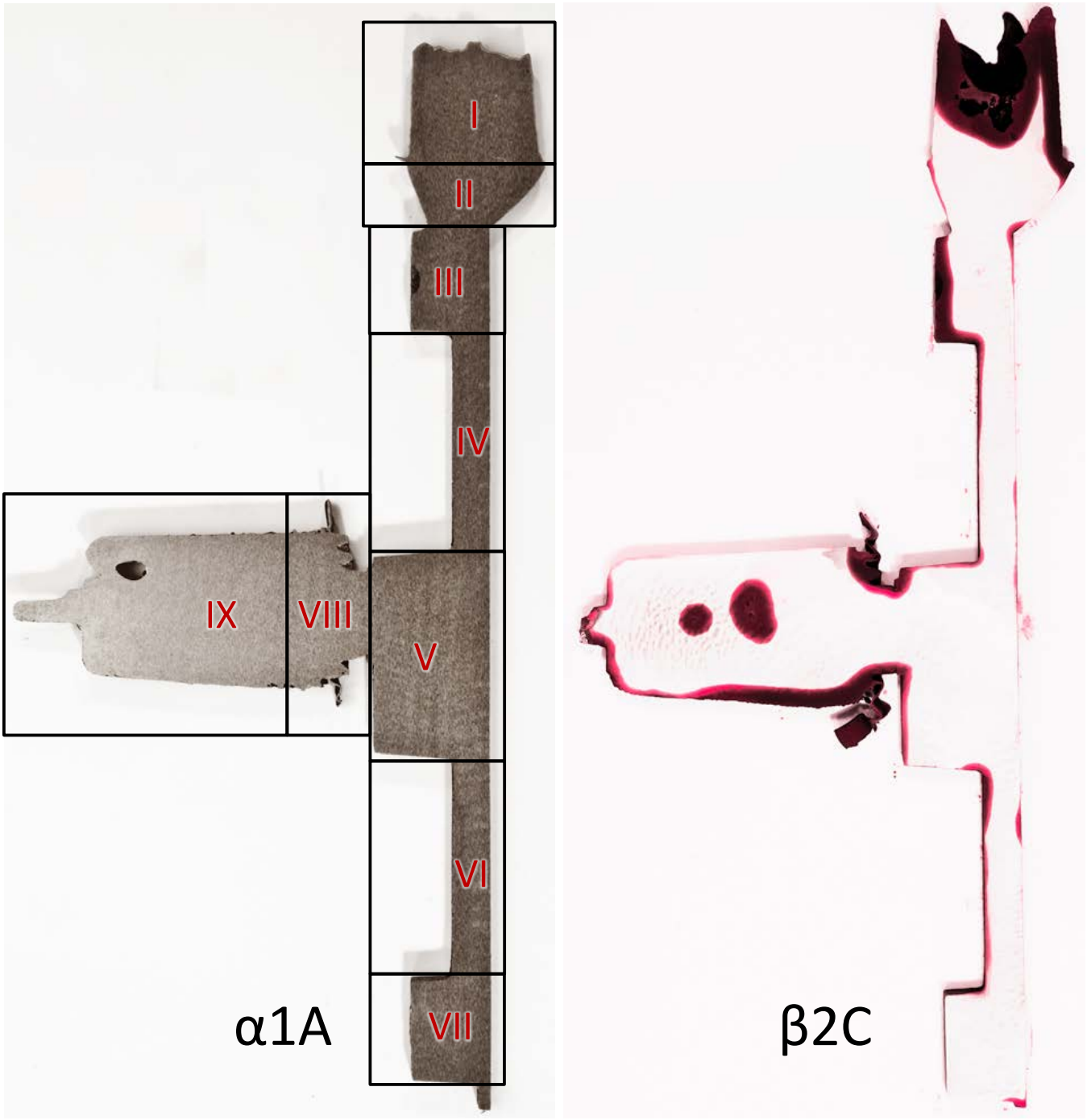

Fig. 3. Left: The 9 non-overlapping areas examined for porosities shown on casting α1A before the liquid penetrant test. Right: Results of liquid penetrant test for casting β2C. Area III is classified with a SP1 defect, and area IX is classified with a CP3 defect.

The castings were separated from the production at the shake-out station, thus to preserve the gating systems intact. Afterwards the castings were shot blast.

LIQUID PENETRANT TEST

All castings were sectioned through the vertical centerline to allow for thorough examination for macro and micro porosities as close to the center as possible. A 5 to 10 mm thick slice was cut from each casting, and the center surface of the slice was then ground to achieve a smooth

surface, see fig. 3. The slices were then etched with oxalic acid dihydrate—approx. 25 g and 500 ml water per casting—at room temperature for 24 h. The etching was done to remove material that the grinding might have smeared over the surface, potentially blocking porosities, thus obscuring the results.

The etched castings were rinsed carefully, then spayed with dye penetrant, allowed to rest for 5-10 min., rinsed again and finally sprayed with the liquid penetrant developer.

All castings were photo-documented within 20 min. of the liquid penetrant development.

The liquid penetrant tests were performed according to European Standard EN 1371-1:2011. The visual evaluation and classification of the porosities also conferred with the descriptions in the standard.

The casting slices were each divided into 9 non-overlapping areas, as seen in fig. 3. Each area was evaluated for size and type of porosities. Also the feeders and feeder necks were evaluated. Porosities are expected in the feeders and do not influence the quality of the casting. Likewise, porosities in the feeder neck do not influence the casting quality, but porosities here indicate that the feeder is close to the limit of its abilities. Thought should then be given to the possibility of choosing a feeder with a higher modulus.

SURFACE DEFORMATION MEASUREMENTS

Insufficient feeding can cause not only porosities, but also surface shrinkage. To be able to evaluate the different feeder combinations influence on surface shrinkage and geometric stability; the plane surface of all castings were measured using a Coordinate Measuring Machine (CMM). The CMM maps the back surface of the castings with a probe, using a pre-programmed measuring layout. A probe with a head diameter of 3 mm was used to ensure a suitable mechanical filter against the roughness of the surface itself. The program ensures identical and comparable measurements between all castings. The 3D-coordinate map is then used to evaluate the flatness of the casting. The flatness value (f_V) is given as a simple measure of the largest difference in height measured across the surface. A perfectly flat surface is equivalent to an f_V of 0.00 mm.

The f_V in itself gives no definite proof of surface shrinkage. Castings can, for various reasons, warp as part of solidification and cooling. However, surface shrinkage will normally exist as a local depression of the surface.

NUMERICAL SIMULATION

All feeder combinations have been simulated and examined using a commercial numerical simulation software—MAGMASOFT 5.2. The simulation setups were configured to mirror the conditions present during the three casting sequences, as best possible.

The simulations were used to evaluate the amount and location of the porosities, and provide the opportunity to see where porosities have a higher probability of forming. Also, porosities located away from the centerline can be identified. Moreover, it is possible to see how porosities develop during solidification, as well as disappear again due to graphite expansion when the casting cools. This is done by analyzing the porosities during solidification in addition to the fully solidified casting.

RESULTS

The castings were evaluated according to several parameters—porosities, porosity location and surface deformation—to properly identify if they would qualify as sound or unsound. As it is not the intent of the present paper to set standards for evaluating sound castings, the defect types are listed for the different areas. The acceptable amount, size and placement of casting defects are very dependent on application.

POROSITIES

Reviewing the 9 areas for all 8 feeder and alloy combinations, all defects were classified as either non-linear isolated indications (SP) or non-linear clustered indications (CP) in accordance to EN 1371-1:2011 (C, D).

Areas II, IV and VI displayed no defect indication for any of the 24 castings. Area II is the feeder neck of the top feeder, and concludes that the top feeder is feeding sufficiently for all castings. Areas IV and VI are the thin walled sections in between the boss and the outer ring. For casting β3C, an SP1 defect was identified for area VII—the bottom ring. For all other of the 24 castings area VII was defect free.

Thus, with focus on the areas III, V and VIII, it is possible to analyze the different feeders' ability to sufficiently feed the casting.

Reference Castings

In order to quantify the effect of the different feeders, reference castings without the feeders were needed. Casting groups α3 and β3 were cast without the center feeder. Casting group α4 was cast without the top feeder, and casting group α5 was cast without either of the feeders.

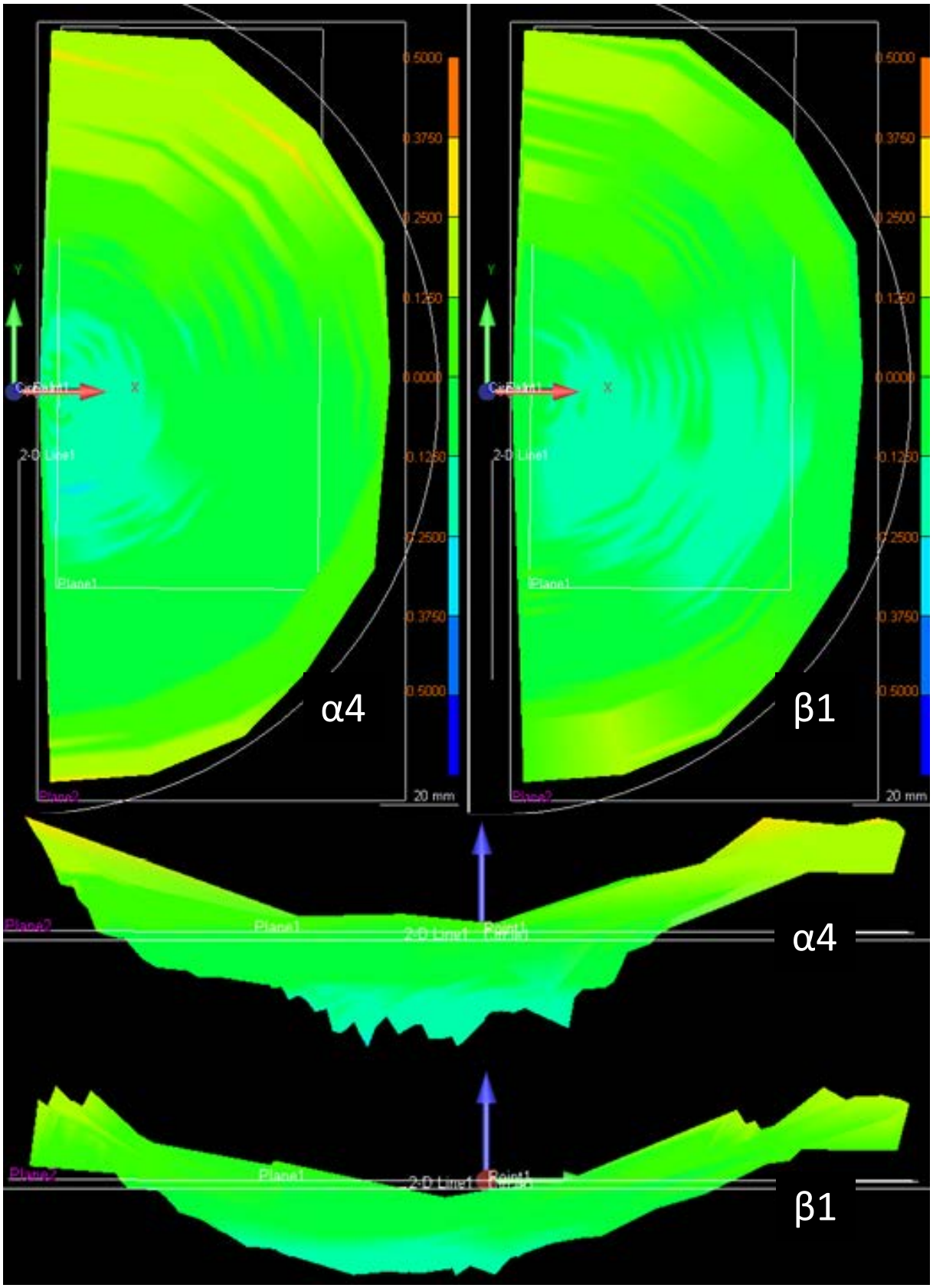

Fig. 4. Flatness of castings α4A and β1A. The halved castings are view from the top and the side. All four representations adhere to the same scale. 0.00 is the mean value and the color scale covers ± 0.50 mm. Note that the warp-effect for both castings are large enough to obscure the effect of surface shrinkage.

Casting group α3 display SP1 or CP1 defects in area V. Casting group α4 display SP1 defects in area III. Castings α5A and C display SP1 and CP1 defects in area III and V, while casting α5B display a SP1 defect in area III. None of the reference castings are without defects. These nine castings are all cast as EN-GJS-500-7 iron.

Casting group β3 is without center feeder—like casting group α3—but as EN-GJS-450-10 iron. All three castings have defects classified as SP1, CP2 or CP3 in areas III and V. Again all reference castings contain defects.

EN-GJS-500-7 Castings

Casting groups α1 and α2 are cast as EN-GJS-500-7 iron with a fairly high graphite precipitation. For the three areas in focus, for all six castings, only the feeder neck—area VIII—for casting α2B displayed an SP1 defect.

EN-GJS-450-10 Castings

Casting groups β1, and β2 were equipped with the same feeders as casting groups α1 and α2 respectively, but cast with a different alloy. For the three areas in focus casting group α1 displays no defects. Casting β2A displays an SP1 defect in area VIII. Casting β2B displays an SP2 defect in area V and an SP1 defect in area VIII. Finally, casting β2C displays an SP1 defect in area III.

The results of the liquid penetrant test are summarized in table 4.

SURFACE DEFORMATION

Of the 24 castings 20 have a flatness value between 0.33 and 0.53 mm with a maximum difference between castings α1B and α2B of 0.2 mm. Casting group α5 has a far greater f_V ranging from 0.82 to 0.97 mm. Casting groups α3 and α4 have comparable flatness values even though they lack either the top or the center feeder. The absence of both feeders about doubles the height difference measured across the surface, compared to all the other castings. See fig. 5.

As shown in fig. 5 there is some difference in flatness related to the combination of feeders used. The exothermic feeders of casting group α1 have an f_V approx. 25% larger than the purely insulating feeders used for casting group α2. The same effect is not seen for the EN-GJS-450-10 alloy where f_V varies between 0.39 and 0.41 mm.

The flatness value, though, cannot directly be linked to surface shrinkage. The variation in height difference across the back surface of the casting can also be related to a warping caused by thermal stresses that occur during cooling, see fig. 4. All castings show warping. It is impossible from the data at hand to conclude how large a part of the surface un-flatness that is shrinkage related. In some castings—like α4A—a low area is located close to the boss, while others—like β1A— show a low area covering the larger part of the middle section of the casting.

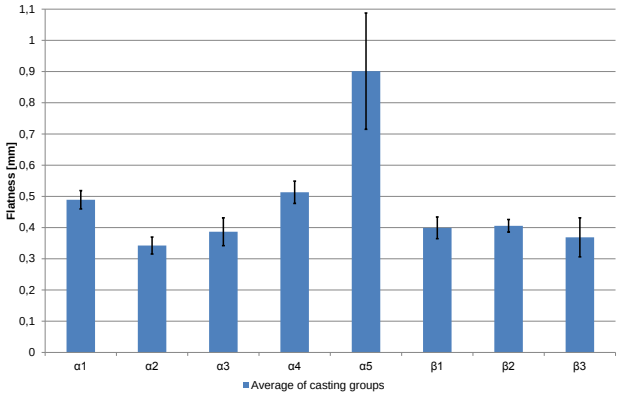

Fig. 5. Flatness Value (f_V) as an average for each casting group, with 95% confidence T interval marked by the error bars.

Another feature observed for all castings are ripples that radiate from the center boss towards the outer ring. The ripples are differences in height, and the height differences between ripple peak and valley are in most cases less than 0.1 mm. Nevertheless, the ripples are present for all castings and do vary slightly with respect to amplitude and wavelength.

SIMULATIONS

Porosity Analysis

Analyses of the porosity formation during solidification show that the main difference between the two alloys is indeed the better recuperation of the EN-GJS-500-7 alloy. This was expected as the EN-GJS-500-7 has a higher C content, and thus a greater graphite expansion, compared to the EN-GJS-450-10.

The simulations show a few areas with possibility for minor porosities. The feeders with exothermic sleeves show areas with intensive porosity formation, indicated by the red and yellow colors in fig. 6-α1. The feeders with insulating sleeves display areas with potential porosity formation, but on a different level than the feeders with exothermic sleeves, indicated by blue in fig. 6-α2.

The changes in alloy also resulted in change to the size and location of the porosities. The EN-GJS-450-10 showed increased tendency for porosities compared to the EN-GJS-500-7, using the same graphite expansion factor. The EN-GJS-500-7 is simulated with a graphite precipitation factor of 8. Simulating several different graphite precipitation factors with the EN-GJS-450-10, and comparing these to the results of the liquid penetrant test, the best matching graphite expansion factor is between 6 and 7. See fig. 6-β1+β2.

Fig. 6. Porosity simulation for casting groups α1, α2, β1 and β2. The 3D model is sectioned through the vertical centerline, exactly as the real castings were. The simulations of α1 and α2 apply a graphite precipitation factor of 8, and the simulations of β1 and β2 apply a factor of 6.

Examining the thermal gradients produced by the different types of feeder sleeves, it is clear that the exothermic and exothermic-insulating sleeves have a significantly higher modulus than the insulating sleeves. See fig. 7.

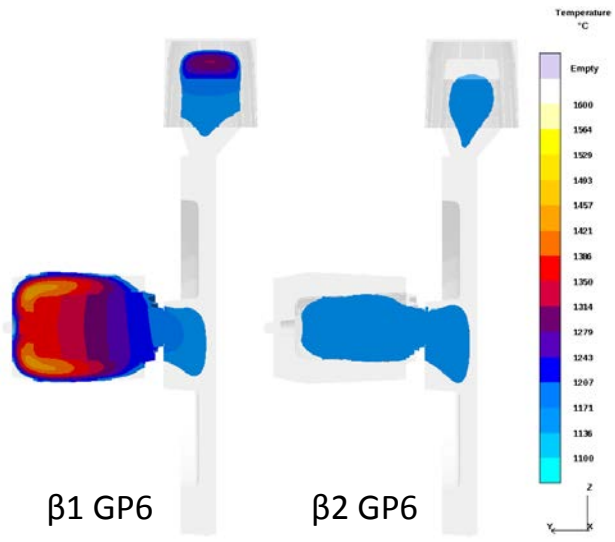

Fig. 7. Simulation of thermal gradients at the center cross-section of the casting, including feeder sleeves. Comparing exothermic and exothermic-insulating sleeves on β1 (left) with insulating sleeves on β2 (right). Both simulations show at 85% solidified.

DISCUSSION

POROSITIES

EN-GJS-500-7

The casting porosity analysis shows almost no defects for casting groups α1, α2 and β1. The one defect identified in these 9 castings is found in α2B area VIII and classified SP1. It is a very small non-linear porosity in the feeder neck of the center feeder. Thus, all 9 castings are sound for all categories according to the EN 1371-1:2011.

Compared to the casting groups α3, α4 and α5, which were cast with the same alloy as above, but cast without one or both feeders, all of these 9 castings display SP1 or CP1 defects in one or more areas. Casting group α3 directly show the effect of not using a spot feeder. α3A and B display SP1 defects at area V, while α3C display a CP1 defect in the same area. As the design of the casting was made to provoke this type of defects, this is not surprising, but it proves that both the exothermic and the insulating spot feeders provide the conditions needed to produce defect free castings. The spot feeders supply melt, heat and pressure sufficient for the boss to be porosity free.

Casting group α4—center feeder and no top feeder—display no defects in area V, but SP1 defects in area III. This corresponds with the intension of the casting design. Likewise, casting group α5 displays SP1 or CP1 defects in area III and V respectively. The only exception is α5B, area V, which is defect free.

Table 4. Summation of results comparing feeder sleeve material (and modulus) with type and size of porosities found in the liquid penetrant test, as well as the flatness value from the CMM measurements. Results for both alloys are shown. Exo = exothermic, Ins = insulating and E/I = exothermic-insulating.

	GJS-500-7															GJS-450-HS								
	α1			α2			α3			α4			α5			β1			β2			β3		
Top Feeder Sleeve Material	E/I			Ins			E/I			N/A			N/A			E/I			Ins			E/I		
Top Feeder Sleeve Thermal Modulus	10 mm			9 mm			10 mm									10 mm			9 mm			10 mm		
Center Feeder Sleeve	Exo			Ins			N/A			E/I			N/A			Exo			Ins			N/A		
Center Feeder Sleeve Thermal Modulus	12 mm			11 mm						11 mm						12 mm			11 mm					
	A	B	C	A	B	C	A	B	C	A	B	C	A	B	C	A	B	C	A	B	C	A	B	C
Areas of the Castings examined for porosities III										SP1	SP1	SP1	SP1	SP1	SP1						SP1			
Areas of the Castings examined for porosities V							CP1	CP1	SP1				CP1		CP1					SP2		CP2	SP1	CP3
Areas of the Castings examined for porosities VIII					SP1														SP1	SP1				

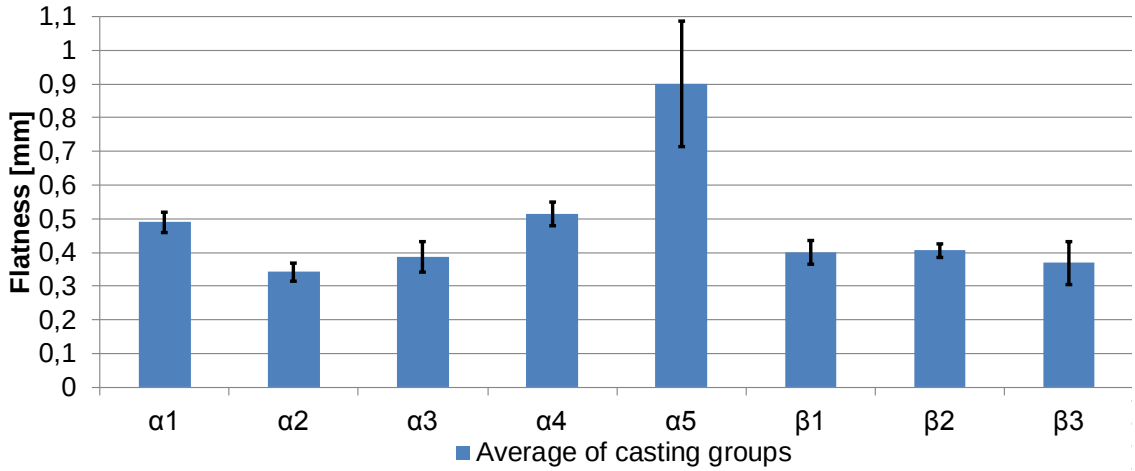

EN-GJS-450-10

The more shrinkage prone, high silicon alloy EN-GJS-450-10, display more severe porosities than the EN-GJS-500-7. Only casting group β1 is defect free. Casting group β1 applies an exothermic/insulating top feeder sleeve, and an exothermic center feeder sleeve. Casting group β2 displays defects, though to a varying degree. Casting β2A display an SP1 defect in area VIII—the center feeder, feeder neck—and the casting itself is thus without defects. This defect is similar to the same area of casting α2B, which is cast with the exact same feeder configuration. The difference is that while α2B displayed the only defect of the whole casting group, β2A is the only casting of the group that is not flawed with defects inside the critical areas. Thus, the EN-GJS-450-10 has shown that there is a functional difference between the insulating and exothermic feeders, where the extended M_t of the exothermic feeder sleeve made all the difference.

Finally, as a reference to casting group α3, casting group β3 tests the effect of an absent center feeder with the EN-GJS-450-10 alloy. As with casting group α3, the affected area is area V. The severity of the defects is just greater than with the EN-GJS-500-7 alloy.

Potential Process Errors

Porosities may as well be located 5 mm away from the centerline of the casting, as it may be exactly where the cut was made. Thus, it is certain that the porosities that are found are there, whereas other porosities may be located just below the surface escaping detection.

The test has been conducted with ground and etched castings to minimize the effects of machining on the castings. It is unlikely that any significant defects were obscured from the liquid penetrant test by this.

Potentially some minor defects may have escaped detection due the choice of photo documenting the castings, rather than evaluating them in quick succession of the penetrant development. Direct evaluation of the castings would have allowed use of a 3X magnification during examination in accordance with EN 1371-1:2011. Even though it cannot be ruled out completely that more defects may have been found, all of these would have been microscopic and probably well outside the detection capabilities of both X-ray and ultrasound. On the other hand the digitalization of the liquid penetrant tests allowed for different digital filters to be used processing the images, enhancing different features of the images,

and thus ensuring that all parts of the images were given the optimum display conditions. Moreover, the digitalization enables continued analysis and allow for several people to review and classify the results.

Finally, the dye on the sides of the casting that was not efficiently rinsed away during the rinsing process, slowly dissipate into the area of interest. Throughout the analysis these false positives have been omitted from the results, but it is possible that small porosities that would normally have been identified, has been obscured by the coloring from the edges. As the porosities are most likely to form at the center of a section, away from the edges, it is less likely that this phenomenon have influenced the results. Albeit, the sections are small, and the edge-penetrant may very well reach parts of the casting that can be expected to have porosities.

Porosity Simulation

The analysis of the porosity formation during solidification showed that the centerline is the most likely place to find porosities for this casting geometry. Though porosities can be located off center, the simulation also shows that these have a size that is unlikely to show up on either X-ray or ultrasound analyses. Especially the bottom part of the outer ring may be prone to these off-center porosities. The simulations show good correspondence with the size and location of the porosities found in the liquid penetrant test.

The analysis of the thermal gradients related to the different feeder sleeves show that the exothermic sleeves not only retain the temperature of the melt for an extended period, it raises the temperature inside the feeder, thus making the thermal gradient steeper than that produced by the insulating feeder sleeves.

SURFACE DEFORMATION

The deformation of the back surface of the casting is expected to have two origins: the shrinkage of the surface due to decreasing volume during solidification and cooling, and the warping of the casting due to thermal stresses deforming the casting during solidification and cooling.

Reproducibility

The measurements show great reproducibility between the different casting groups as can be seen in fig. 5. The 95% confidence interval is overlapping for casting groups α2, α3, β1, β2 and β3. Casting groups α1 and α4 are slightly higher then aforementioned groups, but overlap with each other. The final group—α5—clearly differentiate itself from the other groups. Casting group α5 displays clear signs of surface shrinkage at the back surface of the boss, which adds additional height difference to the already warping surface. Remember that group α5 is the one cast without either of the feeders.

Feeder Interaction

Comparing the surface shrinkage at the boss for casting group α5 with the other groups, casting groups α3 and β3 show interesting results. Neither group α3 nor group β3 displays any great surface shrinkage near the boss. This is interesting because these two groups, like casting group α5, were cast without the center feeder. However, the presence of the top feeder seems to be sufficient to avoid gross surface shrinkage at the center boss. Despite the thermal division caused by the thin walled low modulus section separating the two. Instead the top feeder manages to influence the solidification at the center boss. The influence can come from change to the thermal gradients of the casting or by increased ferrostatic pressure. The authors expect the ferrostatic pressure as the prime influence, albeit more tests are required to conclude to which amount the effect can be contributed to change to thermal gradients or ferrostatic pressure.

It must be noted, though, that the feeding is still not sufficient to a degree that the center feeder can be avoided. Group α3 displays larger and more severe internal porosities at the boss, thus the reduced surface shrinkage do not ensure a sound casting.

Ripples

The surface flatness measurements showed a ripple-like effect radiating as circular waves from the boss at the center, outwards towards the outer ring. All 50 casting part of the experiment display this feature.

As many of the ripple peaks and valleys consist of multiple measurement points, it is highly unlikely that the measurements are coincidental. Moreover, the ripples seem to have fairly the same wavelength depending on feeder combination. Some groups like α1, α2 and α3 display shorter wavelengths, while group α4 displays longer ripple wavelengths.

While the ripples appear to be consistent and linked, the graded color scale used to illustrate the surface flatness also obscure the accuracy of the ripple. The stepwise colors make it impossible to determine the exact height of a given point. Thus two points with the same green color may have a height difference of as much as 0.125 mm, while at the same time two other points—having different colors—may be as little as 0.001 mm apart.

New, more detailed measurements, must be made before conclusions can be drawn, though present results suggest a clear interdependency between modulus and deformation. It seems likely that the ripples are a result of the inner boss, outer ring construction. Determining how different geometries behave during these sinusoidal contractions may help improve dimension stability and give better understanding of how feeder potentially can help change or avoid these features.

CONCLUSION

The experimental castings were made with great reproducibility, and show that the ram-up spot feeders provide sufficient feeding to successfully cast this casting, that is otherwise deemed unsound.

The casting geometry was cast without the center feeder as a reference. This showed porosities at the center boss for all three castings of each alloy. For the EN-GJS-500-7 alloy with a standard ductile iron graphite precipitation, any combination of two feeders proved to produce sound, defect free castings. With the more shrinkage prone EN-GJS-450-10 alloy, only the feeder combination with the high M_t exothermic and exothermic/insulating feeders proved sufficient. The combination with solely insulating sleeves produced only one of the three castings that displayed no defects in the critical areas.

It was found that the top feeder did influence the solidification in the boss area, even though the boss was isolated from the top feeder by the thin walled section in between. Moreover it was also found that the feeder modulus affected the flatness value of the castings back surface, and that the deviation with each casting group was insignificant compared to the overall warp of the casting.

ACKNOWLEDGMENTS

Thanks are due to the funding body of the project; the PSO funds from the Danish government. Moreover, the project comprises the collaborating effort of FOSECO Ltd., MAGMA GmbH, DISA Industries A/S, Vald.Birn A/S and The Technical University of Denmark, department of Mechanical Engineering. All have been engaged in the work and have contributed helpfully to the results presented in this paper.

REFERENCES

1. Tiedje, N.S., “Resource Savings by Optimising Process Conditions in Foundries”, World Foundry Congress (2008)

2. Brown, J.R., “Foseco Ferrous Foundryman’s Handbook,” Foseco International (2000)

3. http://www.ductile.org/didata/section12/12intro.htm (September 2012)